FORMATION FLIGHT AND WAKE VORTEX ENCOUNTERS WITH FULLY COUPLED HYBRID RANS/LES

Anton Stephan[1] and Stefan Zholtovski[2] and Frank Holzäpfel[3]

[1]*DLR Institute of Atmospheric Physics, Muenchener Str. 20, 82234 Oberpfaffenhofen, Germany, anton.stephan@dlr.de*
[2]*DLR Institute of Atmospheric Physics, frank.holzaepfel@dlr.de*
[3]*DLR Institute of Atmospheric Physics, stefan@imperiumdrive.com*

ABSTRACT

The vision of establishing a simulation system for virtual flight in a realistic environment is solved by the coupling of two separate flow solvers in a bi-directional manner, a compressible Reynolds-Averaged Navier-Stokes (RANS) solver and an incompressible Large-Eddy Simulation (LES) solver. It enables the simulation of a flight through realistic atmospheric turbulence, including the effects on the aircraft and the roll-up of trailing vortices and their further development until final decay. This method is applied to aircraft encountering the wake of previous aircraft under different angles of attack, and formation flight as a special case. Moments experienced by the following aircraft are evaluated, the aerodynamics is investigated.

1. INTRODUCTION

In modern computational aerodynamics ambitious aims are set in multiple numerical disciplines, like physical modeling, algorithms, geometry and grid generation and HPC for the next decade [14]. Understanding the complex nature of different interacting scientific spheres, that have been treated independently so far, through novel methods and algorithms, will foster new technologies and innovations in aviation in general. Complex-flight aerodynamics is a profound example of a complex field of physics that covers multiple scales, as complex geometries as well as large domains are of interest that includes multiple disciplines, like aerodynamics, aeroelasticity, meteorology, mashing, wall modeling, etc. Mathematically described by the Navier-Stokes equations, conventional methods are not able to handle the high Reynolds numbers which are characteristic for that kind of problems. High-Reynolds-number wall-bounded flows still cannot be handled by pure turbulence resolving approaches like the large-eddy simulation (LES) or direct numerical simulation (DNS) due to their high grid requirements and the small time steps needed [2]. This will not change in the near future because Spalart's estimate for the availability of a LES of a full aircraft configuration is for the year 2045 [20], even when using wall modeling and assuming Moore's law.

The vision of establishing a simulation system for virtual fight in a realistic environment is solved by the coupling of two separate flow solvers in a bi-directional manner [27]. It enables the simulation of a fight through realistic atmospheric turbulence, including the effects on the aircraft and the roll-up of trailing vortices and their further development until final decay. A compressible Reynolds-Averaged Navier-Stokes (RANS) solver resolves the near-field around a aircraft including its boundary layer. The DLR TAU code that is also used as the in-house code of Airbus is employed for the RANS calculations [17]. An incompressible Large-Eddy Simulation (LES) solver is used to model the atmosphere around the aircraft with its wake footprint in the LES domain. The atmospheric environment is resolved by the structured incompressible LES code MGLET [12]. This method has been validated for the flight through a gust [27] and it is successfully applied to aircraft encountering the wake of previous aircraft under different angles of attack, and formation flight as a special case. Moments experienced by the following aircraft are evaluated, the aerodynamics is investigated. Choosing a hybrid RANS/LES approach we are able to study the wake vortex evolution from roll-up until vortex decay numerically. Hence, we also cover the vortex interaction from the early phase until the complete roll-up.

Wake vortices generated by flying aircraft are highly complex flows due to their three-dimensional unsteady character. The broad range of spatial and temporal scales involved in the different phases of vortex evolution from roll-up to vortex decay make their numerical simulation challenging. On one end of the spectrum lie the scales of the turbulent boundary layer, developing on the aircraft's surfaces, involved in the roll-up process; on the other end are the scales of collective wake-vortex instabilities (e.g. Crow instability [7]) and the eddies of atmospheric turbulence. Several orders of magnitude lie in between. In recent years the investigation of wake vortex could make major progress due to hybrid methods, [22, 23] show applications of an uni-directional coupled RANS/LES approach. In this study we investigate strongly unsteady flight maneuvers with a bidirectionally coupled RANS/LES code.

2. COMPUTATIONAL METHOD - FLOW SOLVERS AND COUPLING MODULE

2.1 RANS solver - DLR TAU code

The Unsteady Reynolds-Averaged Navier-Stokes equations, solved by TAU, are given below:

$$\frac{\partial \bar{\rho}}{\partial t} + \frac{\partial (\bar{\rho} \tilde{u}_j)}{\partial x_j} = 0 \tag{1}$$

$$\frac{\partial \bar{\rho} \tilde{u}_i}{\partial t} + \frac{\partial \bar{\rho} \tilde{u}_i \tilde{u}_j}{\partial x_j} = -\frac{\partial \bar{p}}{\partial x_i} + \frac{\partial \bar{\sigma}_{ij}}{\partial x_j} + \frac{\partial \overline{\rho u_i'' u_j''}}{\partial x_j} \tag{2}$$

In this compressible formulation Favre averaging is used to avoid expressions where products of density and velocity fluctuations appear. The Favre-averaged variables are defined as $\tilde{\phi} = \frac{\overline{\rho \phi}}{\bar{\rho}}$ and the Reynolds decomposition of instantaneous variables reads $\phi = \tilde{\phi} + \phi''$, where ϕ'' is the fluctuating part, for which $\overline{\rho \phi''} = 0$. The overbars denote the usual Reynolds averaging. The system of the compressible RANS equations is closed with the Favre-averaged energy equation, the ideal gas law, Sutherland's law and a fixed turbulent Prandtl number relating the turbulent viscosity to thermal diffusivity. $\bar{\sigma}_{ij}$ denotes the viscous stress tensor, whereas $\overline{\rho u_i'' u_j''}$ is the Reynolds stress tensor, including the contribution of all turbulent scales to the momentum balance. For incompressible flows the energy equation is fully decoupled and as we are not interested in the temperature field, it can be ignored.

A highly accurate, robust and reliable code, capable of handling complex geometries is needed to adequately resolve the boundary layer and the near-field of an aircraft. The DLR TAU code [17], developed at the DLR's Institute for Aerodynamics and Flow Control in Brunswick,

covers these criteria and was chosen for all RANS simulations here. It employs unstructured meshes and can thus handle complex geometries. Various spatial and temporal discretization schemes are available, as well as a variety of solution algorithms and convergence acceleration techniques. A variety of two-equation models and Reynolds stress models are on hand, in addition to the popular Spalart-Almaras one equation model and hybrid RANS/LES models, based on the SA, k-ω and k-ε models.

Given this, TAU is capable of accurately simulating the wake roll-up process, being robust enough despite employing minimal numerical dissipation. The dissipation being low is a needed feature in order to preserve the vorticity shed behind the vortex generator (wing or full aircraft configuration) and transfer it to the LES code, which then handles its evolution in the atmosphere.

Aiming for a robust, but still low dissipation setup, we employ a matrix dissipation scheme [24], as well as the robust, but accurate Spalart-Almaras turbulence model [18]. A rotation correction (RC), based on the original proposal by Spalart and Shur [19], is applied to the SA model to help preserve the wake-vortex cores in the RANS-regions. Braun found [5] that the SA-RC model delivers good results in the near-field of the vortex generator, even compared to different Reynolds Stress models, which are mostly numerically unstable. Different multigrid cycles were employed to accelerate convergence, in addition to a low Mach number preconditioning for some cases with particularly low Mach number. A second-order accurate dual time stepping scheme is employed [11], which practically removes the time step constraint in the unsteady coupled simulation, at least for the RANS part.

2.2 LES solver - MGLET

Filtering the Navier-Stokes equations in space (can be seen as volume averaging), leads to the system of equations solved by the LES code:

$$\frac{\partial \hat{u}_i}{\partial x_i} = 0 \tag{3}$$

$$\rho \frac{\partial \hat{u}_i}{\partial t} + \rho \frac{\partial \hat{u}_i \hat{u}_j}{\partial x_j} = -\frac{\partial \hat{p}}{\partial x_i} + \mu \frac{\partial^2 \hat{u}_i}{\partial x_j x_j} - \rho \frac{\partial}{\partial x_j} \left(\widehat{u_i u_j} - \hat{u}_i \hat{u}_j \right) \tag{4}$$

where the hat symbol is used to denote spatially averaged quantities. The term $\left(\widehat{u_i u_j} - \hat{u}_i \hat{u}_j \right)$ denotes the subgrid turbulence stresses to be modeled by the LES model. The most important requirements for an LES code are, again, low numerical dissipation, as well as high spatial accuracy and an adequate subgrid-scale model. MGLET, a code developed by the research group of Prof. Manhart at TU Munich [12], was identified as a good solver
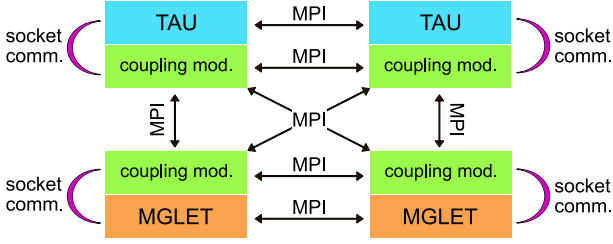
Figure 1: Communication pattern between solvers and coupling module. Simplified figure with one solver process per compute node.

Figure 2: Overview of the LES domain (every 16th grid-line shown) with the RANS domain inside (NACA0012 surface mesh in red). The grey arrow shows the direction of movement of the RANS domain.

for our purposes, mainly due to its fourth-order compact finite-volume spatial discretization scheme [10] [9], as well as the dynamic Lagrangian subgrid-scale model [6], which eliminates the need for calibration. It is an incompressible finite-volume code, employing structured staggered grids, which results in reduced numerical dissipation. The time integration is done explicitly using a three-step Runge-Kutta scheme, which imposes strict limits on the time step. For the Poisson equations a standard velocity-pressure iteration derived from the Newton's method is used [8]. In [4] it is shown that in case of second-order discretization of the divergence terms and the Laplace operator the iteration equations can also be derived from a Gauss Seidel method. That algorithm is performed on four grid levels in a classical multi-grid approach. It is important to mention that compressibility effects are not relevant for the wake-vortex evolution in the atmosphere, which justifies the use of an incompressible solver.

2.3 Code coupling

The communication between both flow solvers is done using a coupling module, currently part of the development release of TAU in version 2017.1. In addition to handling the communication between the solvers, it is also responsible for all search and interpolation procedures. The code communication pattern is shown in Figure 1. Both flow solvers and the coupling module run in parallel using Message Passing Interface (MPI) to communicate with their own processes. The cross-communication between the solvers and the coupling module is realized using socket connections over the Transmission Control Protocol (TCP). For every solver process, a process of the coupling module is pinned on the same computing node, which keeps the socket communication within this node, even if the solver processes span multiple racks or islands of the High Performance Computer used for the coupled simulation. Trilinear interpolation was used when interpolating flow data between solvers. More details about the coupling module can be found in [21].
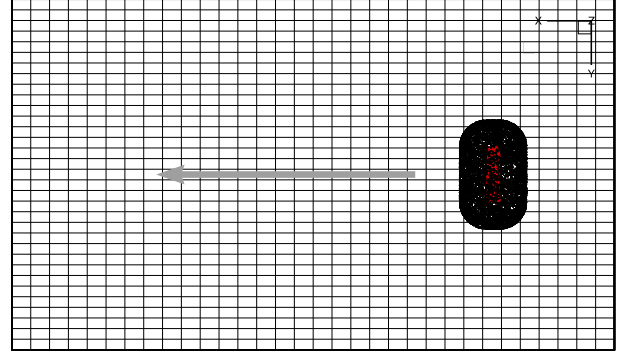
3. COMPUTATIONAL METHOD - SETUP AND INTERFACES

3.1 Simulation setup

Two flow regions can be identified in the hybrid computational setup we employ - the near field of the vortex generator (in general a full aircraft configuration), handled by TAU in RANS mode, and the surrounding atmosphere, handled by MGLET in LES mode, see Fig. 2. The studies presented in the current paper do employ a rather simple wing geometry (a rectangular wing with a NACA0012 profile and blunt wing tips - see Figs. 3, 4, 5). The LES domain is fixed in space and the vortex generator is translated in it, exchanging boundary conditions with it at every physical time step. Note that using an incompressible LES solver is justified here, since the compressibility effects are limited to flow regions in the boundary layer and eventual shocks at higher Mach numbers, which only appear in the compressible RANS domain. Both the RANS and the LES solver have the same physical time step size, limited by the maximal CFL number in the LES domain, as well as the time-scale separation needed in unsteady RANS simulations [26].

All external boundaries in the LES region employ a periodic boundary condition, which provides a minimal boundary interference for the spatially stationary LES domain. The RANS region is embedded within the LES region at all times, in order to ensure that interpolation source points will be found for all interface boundary nodes at all times. The RANS near-field will be located at one domain end in the beginning of the simulation and it will be translated in flight direction until it almost reaches the opposite domain boundary, all the while exchanging boundary conditions based on the Chimera technique for overset grids [3].

The chimera boundary points in the RANS domain, where values are interpolated from the LES domain,
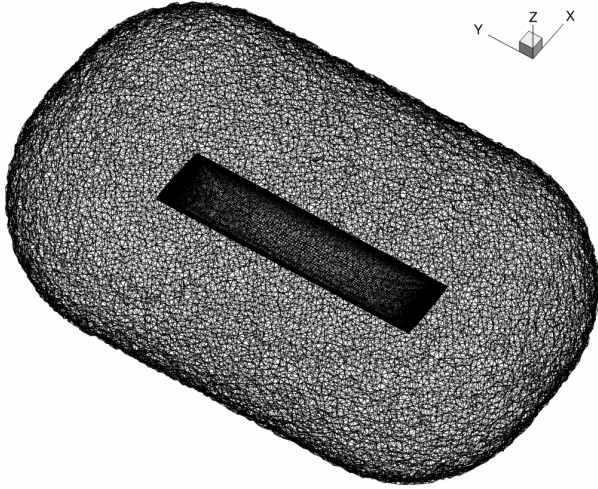
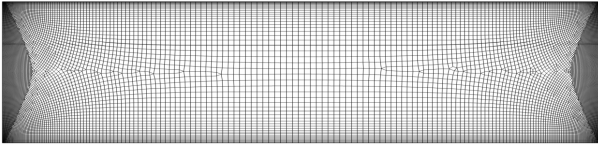Figure 3: RANS mesh with a NACA0012 wing

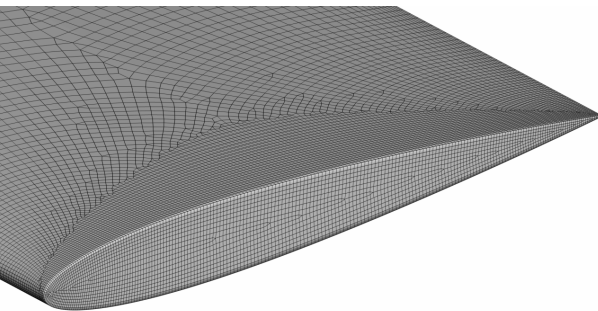Figure 4: NACA0012 - surface mesh (RANS domain), top view

Figure 5: NACA0012 wing tip - surface mesh

lie on its outer surface. In the LES domain, a classic Chimera hole-cutting geometry defines the points to be excluded from the computation and the points to be interpolated from the RANS domain. The latter lie on the outside of the hole-cutting geometry and span several layers outward from the points that intersect the hole-cutting geometry. As it is always the case in Chimera simulations, enough overlap has to be ensured between both grids, but here special attention is given when specifying the LES points that receive data from the compressible RANS domain. It is essential that these points lie outside regions where compressibility effects are dominant, like shocks or high Mach numbers within the boundary layer. The overlap region in the present hybrid simulation needs to be bigger than the overlap region in a pure RANS simulation. We found that MGLET with its compact fourth-order space discretization scheme needs three layers of boundary points at the fringe of the hole-cutting geometry. Decreasing this number degrades accuracy, whereas increasing it does not improve on it. However, for stability reasons additional communication layers should be used in most cases.

Prior to the coupled URANS-LES simulation a steady-state solution is needed for the RANS domain. It is computed in a precursor pure RANS simulation, using an additional background mesh surrounding the near-field around the vortex generator. At the beginning of the coupled transient simulation a pair of straight vortices with the same characteristics as generated by the wing is used as initial condition in the LES domain.

3.2 Interface boundary conditions

Core elements of the two-way coupling method presented in this paper are the interface boundary conditions, where values are interpolated between the flow solvers.

3.2.1 Coupling incompressible and compressible domains

Coupling Low Mach number solvers with a compressible solver was previously investigated by Peet and Lele [16], including the limit $Ma \to 0$ (incompressible flow). The coupling was, however, only employed for laminar cases. Different interface conditions were tested, including three methods where flow variables were directly exchanged (injected) and two methods based on Riemann invariants. Peet and Lele found that the best method in terms of accuracy and stability was also the simplest, where direct injection of the three velocity components, the density and temperature is employed as a boundary condition for both the low-Mach number solver and the compressible solver. In the incompressible limit $Ma \to 0$ the temperature and density fields are constant in the incompressible domain, and they are equal to the free-stream values in

4

the compressible domain. In this study we also employ this direct variable injection (DVI).

3.2.2 Coupling RANS and LES

The occurring problem is related to the different turbulence treatment in TAU and MGLET. Both RANS and LES rely on a scale separation operator, which is, however, rarely known. RANS velocities can be seen as smooth time-averages and contain no turbulence at all, whereas LES velocity fields are <u>instantaneous</u> quantities and also contain turbulence that can be resolved on the computational grid. This implies that, strictly speaking, turbulent content, matching the RANS turbulence statistics, should be added to the communicated velocity fields from RANS to LES. In the one-way coupling approach [13], random white-noise fluctuations, matching the turbulent kinetic energy in the RANS domain, were superimposed to the communicated velocities. However, since the long lifetime of wake vortices is related to their laminar cores, any excess turbulence might lead to unphysical accelerated vortex decay. This is why in the present study the RANS eddy viscosity was completely ignored on the LES side, assuming that turbulence will develop naturally from the resolved velocity gradients, transferred from the finer RANS grid to the coarser LES grid. Any delay in this development is better than over-predicting the real turbulence statistics. This constitutes a conservative approach when vortex decay is being studied.

On the other hand, spectral turbulence content is not resolved in a RANS simulation, which makes an averaging procedure a good way to filter it out from the LES fields and calculate appropriate RANS statistics from it. This averaging is realized by a weighted merging of the instantaneous velocity and the current running average at every grid cell, using an exponential bias-corrected averaging window:

$$u_{i,LES,avg} = \frac{\beta u_{i,LES} + (1-\beta)u_{i,LES,avg}}{1-\beta^{i_t}} \quad (5)$$

where i_t is the time step number. The $1-\beta^{i_t}$ term in the denominator diminishes the bias of the average for small time step numbers. It is only relevant for the first time steps of the simulation, where the predicted average would be underestimated otherwise. We found that $\beta = 0.13$ works well for most cases.

3.2.3 Complete set of interface boundary conditions

Figure 7 shows the LES-to-RANS and the RANS-to-LES interfaces. The LES-to-RANS interface is the outer surface of the RANS domain, which is located 3 chord lengths from the nearest wall of the moving object (the wing or the aircraft). In the cases discussed in this study, the RANS-to-LES interface lies at a cuboid (green surface in Fig. 7), which defines the hole-cutting geometry
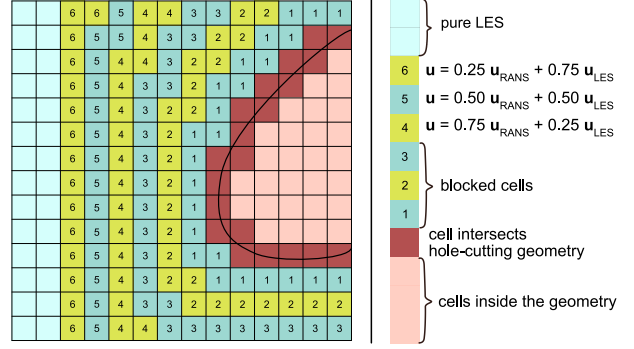

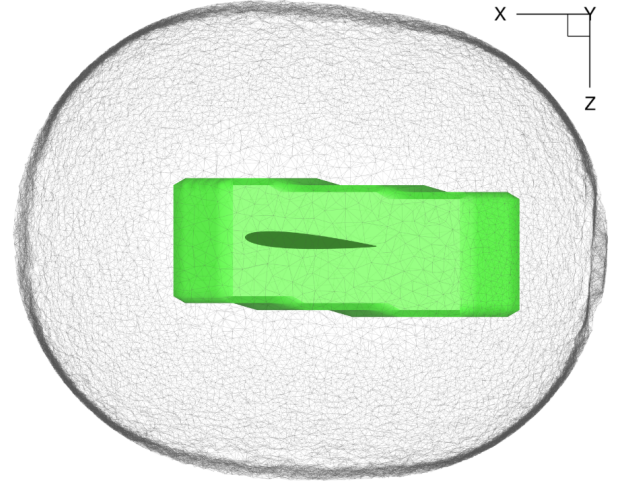Figure 6: Communication points in the LES mesh and blending of RANS and LES data

Figure 7: RANS-to-LES interface in green. LES-to-RANS interface in black on the outer surface of the RANS mesh.

and communication points shown in Fig.6. It is important that all compressible effects occur within the volume bounded by this interface. The boundary layer thickness δ should be small compared to the distance of the object. Still the coherent structures from the RANS simulation should not be dissipated. Due to the small Mach number we do not have transition effects like shock waves.

The RANS-to-LES interface conditions present a direct variable injection (DVI) for all velocity components and the pressure, as illustrated in Fig. 6. The set of LES-to-RANS boundary conditions is as follows:

$$u_{i,RANS} := u_{i,LES,avg} \quad (6)$$
$$p_{RANS} := p_{diff} + dp_{LES} \quad (7)$$
$$\rho_{RANS} := \rho_{LES} = const \quad (8)$$
$$v_{t,RANS} := v_{t,LES} \quad (9)$$

where $p_{diff} = p_\infty - p_{ref,LES}$ is the difference between the free stream reference pressure and the reference pres-

sure in the LES domain (the volumetric average over the whole LES domain or a fixed reference point where the pressure is expected to be close to the freestream pressure for all time steps). dp_{LES} is the pressure calculated in the LES.

4. RESULTS

4.1 Lateral vortex encounter

A lateral vortex encounter is analyzed in this section. Fig. 8 (a) - (c) depicts different instances of the flow field evolution qualitatively. The vorticity magnitude isosurface shows the initialized vortex pair and the flying wing crossing the vortex pair at an angel of 90°, Fig. 8 (a). The moments experiences by the flying wing are depicted in Fig. 9. Fig. 9 (a) is showing the effect on lift - and drag coefficients, while Fig. 9 (b) depicts the evolution of pitching moment (magenta), rolling moment (orange) and yawing moment (green). It should be noted that the LES flow field is not compatible with the RANS field in the first time steps of the coupled simulation and this is why we observe oscillations in the lift coefficient, see Fig. 9 and a starting vortex along with other two-dimensional vorticity structures in the beginning of the LES domain, see Fig. 8 (a). The equilibrium state is achieved shortly after initialization, the oscillating lift and drag coefficient curves converge to the characteristic value, known from the pure steady RANS simulation. Crossing the lateral vortex pair leads to a transition of the lift - and drag coefficient according to the velocity profile generated by the vortex pair. First, the wing experiences an upward motion, leading to an increase in lift and decrease in drag. Note that the first vortex is smeared out, leaving merely a vorticity sheet due to lift change of the wing in that area, Fig. 8 (b). In the downwash region the lift is strongly reduced, even below the initial levels, whereas the drag increases Fig. 9 (a). Finally, the wing leaves the downwash area, flying into the upwash field and finally leaving the vortex bubble. The moments behave accordingly, yet again slightly oscillating before reaching the equilibrium state. Again, the second vortex is smeared out, leaving merely a vortex sheet originating in the lift change of the maneuver, Fig. 8 (c), also observed in [1]. While roll and yaw is constantly zero, we have a pitch evolution corresponding the experienced double vortical gust, Fig. 9 (b), similar to the evolution of drag. Interestingly, the initialized vortices merge with the wing tip vortices, forming a quite unusual vortex pattern, where a vortex end is linked to straight vortex line, Fig. 8 (c). It would be interesting to observe how this pattern develops in time. Though our simulation environment is able to continue that simulation, we have mot performed it yet.

4.2 Encounter from above

Encountering a vortex from above the wing experiences a permanent downwash, yet not constant and not equally distributed along the wing, see Fig. 8 (d). This leads to reduction of lift right from the beginning of the simulation, Fig. 9 (c). At the level of the initialized vortex pair the decline of lift reverses, increasing back to the initial values. Note that the drag is also slightly reduced, while the pitching moment increases during that maneuver, Fig 9 (d). The slight decline in the rolling moment is unphysical and stems from the not perfectly aligned initialization of vortex pair and wing position. Interestingly, after passage the initial vortex pair merge with the wing tip vortices, since both have the same rotation direction Fig. 8 (f).

4.3 Encounter from below

The a similar situation compared to the previous section occurs when the wing is crossing the wake vortex pair from below. Encountering a vortex from below the wing experiences a permanent downwash, yet not constant and not equally distributed along the wing, see Fig. 8 (g). This leads to reduction of lift right from the beginning of the simulation, Fig. 9 (e). The decline of lift reverses, increasing back to the initial values, albeit later than in the case before. Again, the drag is also slightly reduced, while the pitching moment increases during that maneuver, Fig 9 (f). After passage the initial vortex pair merge with the wing tip vortices, Fig. 8 (i).

4.4 Formation flight

Formation flight is gaining more and more attention in air traffic management, as a routing option for saving fuel by decreasing aircraft drag [15]. However there is not much knowledge what does the aerodynamic and the wake of a formation flight look like. This would answers what are optimal formation clusters and how turbulence affects the aircraft positions. Contrail may form contrail cirrus clouds that have a radiation effect, determining the net climatological effect of aviation. The wake evolution is the decisive open question to estimate the contrail formation and evolution [25], since the simulations are very sensitive to initial vortex position.

Though the formation flight can formally be categorized as a vortex encounter and the simulations method is essentially the same, the aerodynamic characteristics change crucially. First let us investigate the flow field qualitatively. Fig. 10 (a) shows the footprint of a wing that flew through the entire domain. Note the opposite rotation direction of the wing tip vortices, colored by red and blue. The starboard wing tip of the following wing is aligned with the vortex center of the port vortex of the leading wing. The following wing smears out the port

(a) before lateral encounter

(b) during lateral encounter

(c) after lateral encounter

(d) before encounter from above

(e) during encounter from above

(f) after encounter from above

(g) before encounter from below

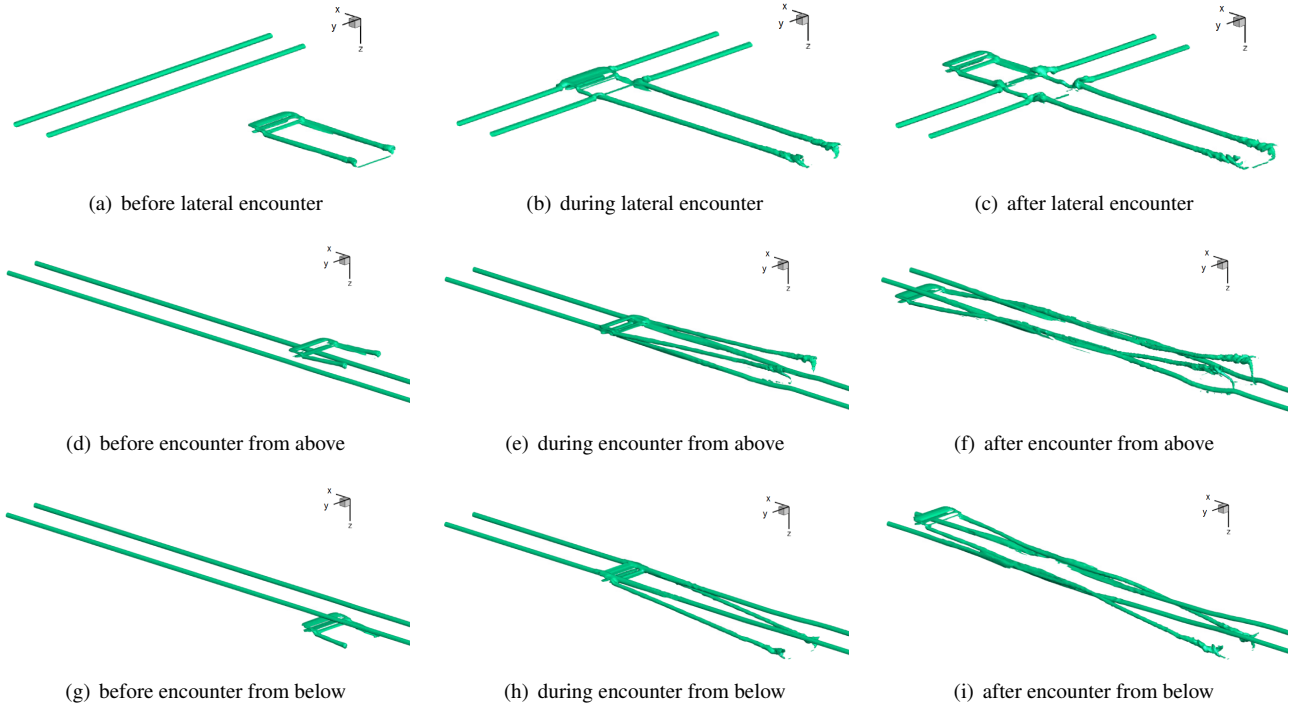(h) during encounter from below

(i) after encounter from below

Figure 8: Vorticity magnitude iso-surface before, during and after vortex encounter, lateral encounter (a) - (c), encounter from above (d) - (f), from below (g) - (i).

vortex of the leading wing, Fig. 10 (b). Finally, the system of the two wings leaves a vortex system of three vortices, one port vortex and two starboard vortices rotating in opposite direction. This information can be used to initialize contrail simulations, to estimate the effect of formation flight on climate. The aerodynamic moments of formation flight are depicted in Fig. 11. After oscillations converged, we observe that the impact of the vortex leads to an increase in lift and a decrease of drag, compared to the steady state (black line). The pitching moment is slightly affected, whereas the rolling moment experiences a strong increase due to the upwash experienced by the wing, Fig. 11.

The physical interpretation of the simulation setup is as follows. Since the following wing does not change the flight path according to the experienced moments, these moments have to be balanced by the weight distribution of the leading wing. This means, for the simulation to be physically valid, the following wing needs to be heavier and the center of gravity needs to be shifted to the right. Indeed, in real applications it is a discussed solution to balance the rolling moment a leading aircraft gets through "surfing" a wake by managing the weight, instead of counter steering with rudder. This solution is more effective in terms of drag.

5. CONCLUSION

In this study we analyzed the physics of different wake encounter scenarios with a fully coupled hybrid RANS/LES approach, with formation flight as a special case. The numerical method was recapitulated and the simulation setup was discussed. We presented the main features of the flow field, as well as the evolution of the lift - and drag coefficients, and rolling - , pitching -, and yawing moments, of the unsteady flight maneuvers. The main findings in the lateral crossing case are that the vortex structures of the initializes vortex pair are smeared out by the wing, leaving a quite surprising vortex pattern where a loose end of a vortex is linked to straight vortex. The moments in this case clearly follow the expected vertical velocity pattern initialized by the vortex pair. Vortex crossing from above and below show quite similar results, dominated by the flight in a downwash region. Interestingly the wingtip vortices merge with the initialized vortices during their generation. Formation flight simulations revealed, that the wake of two wings, flying in a formation is essentially a vortex system of three vortices, two of which have the same sense of rotation. The lift is increased while the drag is reduced. In addition to the always present pitching moment the following wing experiences a significant rolling moment. The method allows to proceed the simulations to larger times, to analyze the evolution of the identified vortex pattern, what will be done in a next step.
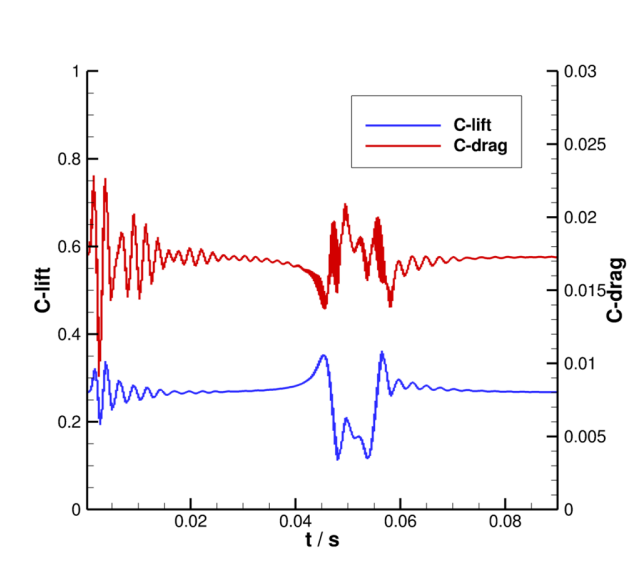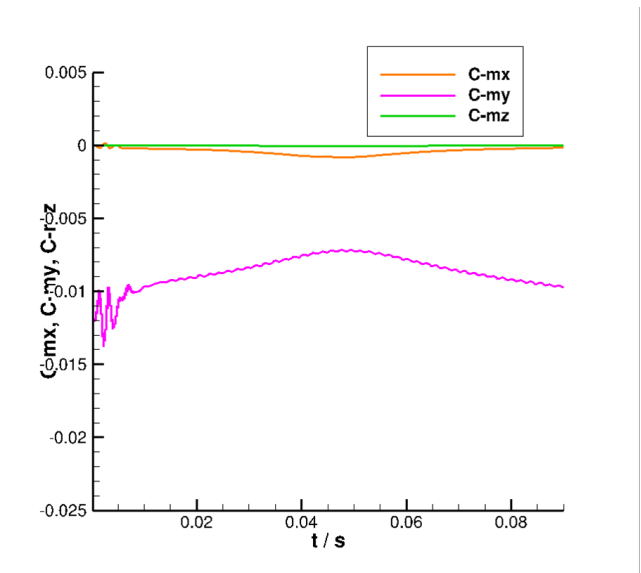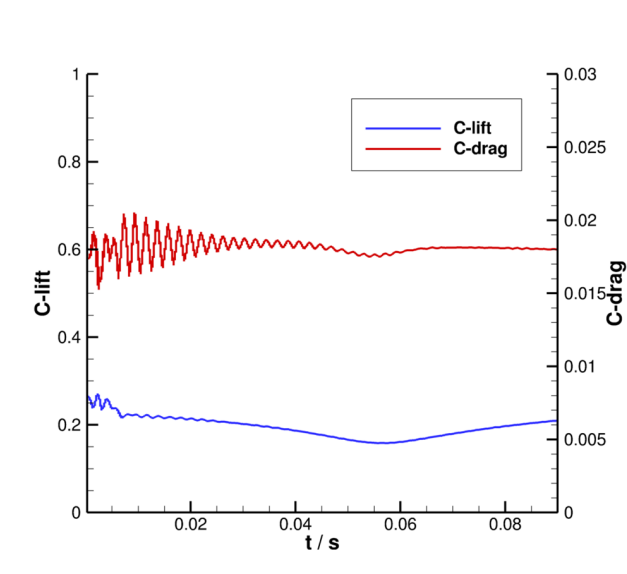
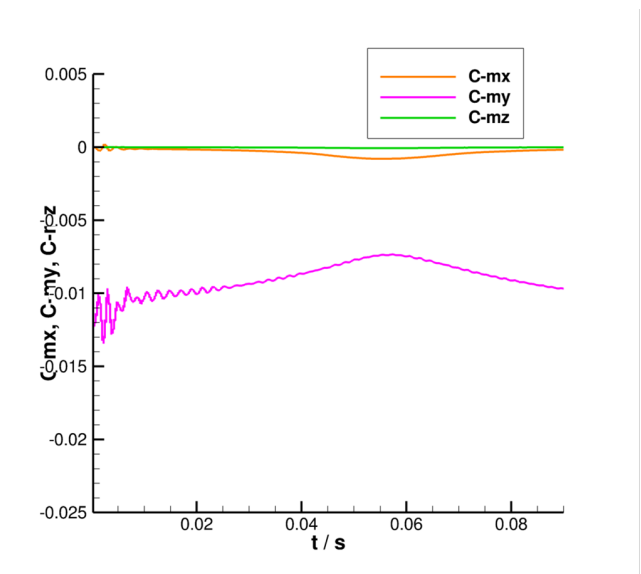(a) lift - and drag coefficient
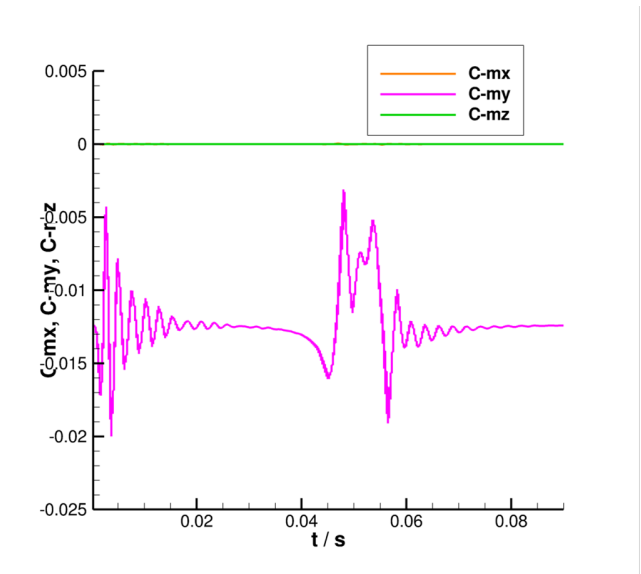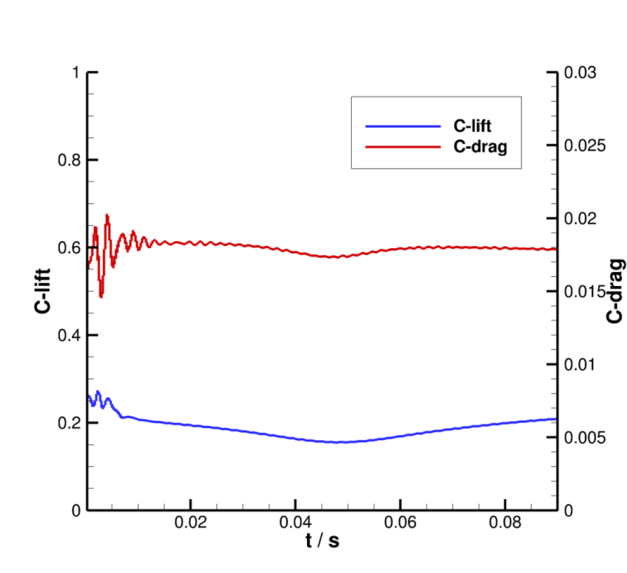
(b) rolling moments

(c) lift - and drag coefficient

(d) rolling moments

(e) lift - and drag coefficient

8

(f) rolling moments

Figure 9: Moments characterizing a lateral vortex encounter (a), (b), encounter from above (b),(c) and encounter from below (e), (f).
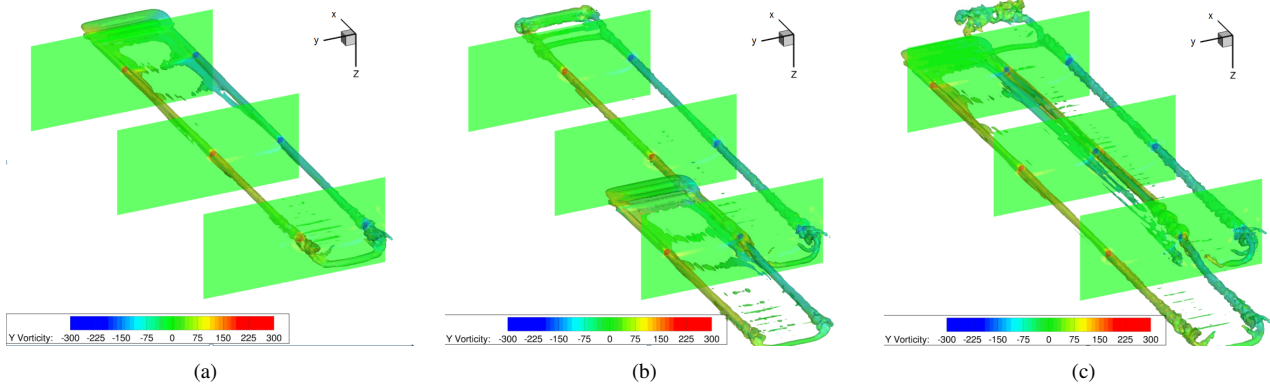
Figure 10: Axial vorticity magnitude in different perpendicular slices, iso-surface of vorticity, in formation flight configuration.

ACKNOWLEDGEMENTS

REFERENCES

[1] C. J. Barnes and M.R. Visbal. Further investigation on the effect of sweep on parallel vortical-gust/wing interactions on a finite aspect-ratio wing. In AIAA AVIATION Forum 17-21 June 2019, Dallas, Texas AIAA Aviation 2019 Forum, 2019.

[2] A. Bechmann and N. N. Sørensen. Hybrid rans/les method for wind flow over complex terrain. Wind Energy, 13(1):36–50, Jan 2010.

[3] J. Benek, J. Steger, and F.C. Dougherty. A flexible grid embedding technique with application to the euler equations. 6th Computational Fluid Dynamics Conference Danvers, Jul 1983.

[4] A. Brandt, J. E. Dendy, and H. Ruppel. The multigrid method for semi-implicit hydrodynamics codes. Journal of Computational Physics, 34:348–370, 1980.

[5] Sebastian Braun. Numerische Simulation von Wirbelaufrollvorgängen an Tragflügeln. PhD thesis, RWTH Aachen, 2016.

[6] William H. Cabot Charles Meneveau, Thomas S. Lund. A lagrangian dynamic subgrid-scale model of turbulence. Journal of Fluid Mechanics, 319:353–385, 1996.

[7] S. C. Crow. Stability theory for a pair of trailing vortices. AIAA Journal, 8(12):2172–2179, Dec 1970.

[8] C. W. Hirt and J. L. Cook. Calculating three-dimensional flows around structures and over rough terrain. Journal of Computational Physics, 10:324, 1972.

[9] Arpiruk Hokpunna. Compact fourth-order scheme for numerical simulations of Navier-Stokes Equations. PhD thesis, Technical University of Munich, 2009.

[10] Arpiruk Hokpunna and Michael Manhart. Compact fourth-order finite volume method for numerical solutions of navier–stokes equations on staggered grids. Journal of Computational Physics, 229(20):7545–7570, Oct 2010.

[11] A. Jameson. Time dependent calculations using multigrid, with applications to unsteady flows past airfoils and wings. In AIAA 10th Computational Fluid Dynamics Conference, 1991.

[12] Michael Manhart. A zonal grid algorithm for dns of turbulent boundary layers. Computers and Fluids, 33(3):435–461, Mar 2004.

[13] Takashi Misaka, Frank Holzapfel, and Thomas Gerz. Wake evolution of high-lift configuration from roll-up to vortex decay. 51st AIAA Aerospace Sciences Meeting including the New Horizons Forum and Aerospace Exposition, Jan.

[14] NASA. Nasa, cfd vision 2030 study, a path to revolutionary computational aerosciences. Technical Report NASA/CR-2014-218178, NASA, https://ntrs.nasa.gov/search.jsp?R=20140003093 2019-06-24T12:09:31+00:00Z, 2014.

[15] A. Ning, T.C. Flanzer, and I.M. Kroo. Aerodynamic performance of extendedformation flight. Journal of Aircraft, 48(3):855–865, May 2011.

9
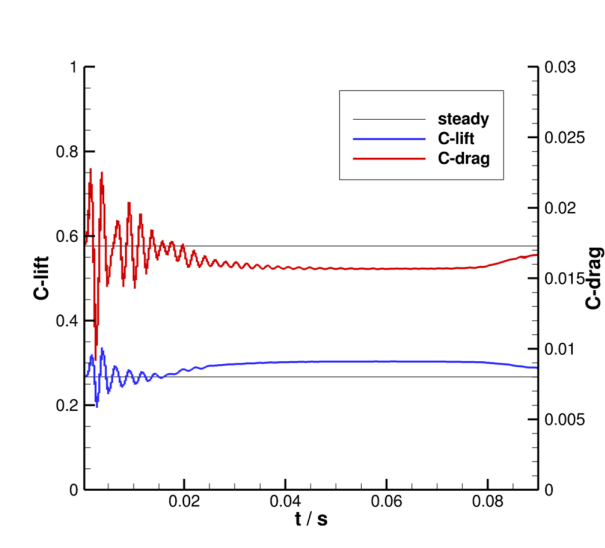
(a) lift - and drag coefficient
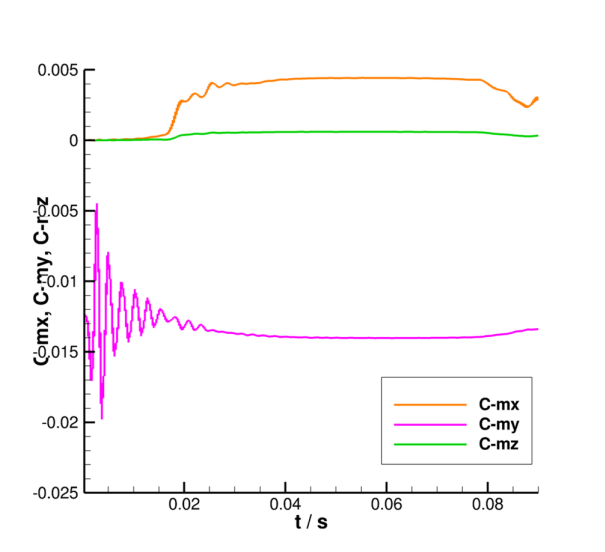
(b) rolling moments

Figure 11: Moments characterizing formation flight.

[16] Y. V. Peet and S. K. Lele. Computational framework for coupling compressible and low mach number codes. AIAA Journal, 46(8):1990–2001, Aug 2008.

[17] Dieter Schwamborn, Thomas Gerhold, and Ralf Heinrich. The DLR TAU-code: Recent applications in research and industry. In European Conference on Computational Fluid Dynamics, 2006.

[18] P. Spalart and S. Allmaras. A one-equation turbulence model for aerodynamic flows. 30th Aerospace Sciences Meeting and Exhibit, Jan 1992.

[19] P. R. Spalart and M. Shur. On the sensitization of turbulence models to rotation and curvature. Aerospace Science and Technology, (5):297–302, 1997.

[20] P.R. Spalart. Strategies for turbulence modelling and simulations. International Journal of Heat and Fluid Flow, 21:252–263, 2000.

[21] F. Spiering. Coupling of tau and trace for parallel accurate flow simulations. In International Symposium on Simulation of Wing and Nacelle Stall, Braunschweig, 2012.

[22] Anton Stephan, Frank Holzapfel, and Takashi Misaka. Hybrid simulation of wake-vortex evolution during landing on flat terrain and with plate line. International Journal of Heat and Fluid Flow, 49:18–27, October 2014.

[23] Anton Stephan, David Rohlmann, Frank Holzpfel, and Ralf Rudnik. Effects of detailed aircraft geometry on wake vortex dynamics during landing. Journal of Aircraft, 56(3):974–989, 2019.

[24] R. C. Swanson. On central-difference and upwind schemes. Journal of Computational Physics, 101:292–306, 1992.

[25] S. Unterstrasser and A. Stephan. Far field wake vortex evolution of two aircraft formation flight and implications on young contrails. The Aeronautical Journal, 1:1–36, 2020.

[26] David C. Wilcox. Turbulence Modeling in CFD. DCW Industries, 3. edition, 2006.

[27] Stefan Zholtovski, Anton Stephan, and Frank Holzpfel. Towards virtual flight in realistic environments: A hybrid coupled simulation method. AIAA Journal, 0(0):1–12, 2020.